Monthly Notices
of the
ROYAL ASTRONOMICAL SOCIETY

Mon. Not. R. Astron. Soc. **402,** 1767–1779 (2010) doi:10.1111/j.1365-2966.2009.15999.x

X-ray emission characteristics of two Wolf–Rayet binaries: V444 Cyg and CD Cru

Himali Bhatt,[1]★ J. C. Pandey,[1] Brijesh Kumar,[1] K. P. Singh[2] and Ram Sagar[1]

[1]*Aryabhatta Research Institute of Observational Sciences, Manora Peak, Nainital 263 129, India*
[2]*Tata Institute of Fundamental Research, Mumbai 400 005, India*

Accepted 2009 November 5. Received 2009 November 5; in original form 2009 July 31

ABSTRACT

Using data from observations made with *XMM–Newton*, we present an X-ray analysis of two Wolf–Rayet (WR) binaries: V444 Cyg and CD Cru. The X-ray light curves show the phase-locked variability in both binaries, where the flux increased by a factor of ∼2 for V444 Cyg and ∼1.5 for CD Cru, from minimum to maximum. The maximum luminosities in the 0.3–7.5 keV energy band were found to be 5.8×10^{32} and 2.8×10^{32} erg s^{-1} for V444 Cyg and CD Cru, respectively. The X-ray spectra of these stars confirmed large extinction and revealed hot plasma with prominent emission-line features of highly ionized Ne, Mg, Si, S, Ar, Ca and Fe; these are found to be consistent with a two-temperature plasma model. At a temperature of ∼0.6 keV, the cooler plasma was found to be constant at all phases for both binaries, which could be the result of a distribution of small-scale shocks in radiation-driven outflows. The hot components in these binaries were found to be phase-dependent. They varied from 1.85 to 9.61 keV for V444 Cyg and from 1.63 to 4.27 keV for CD Cru. The absorption of the hard component varied with the orbital phase and was found to be maximum during the primary eclipse of V444 Cyg. The high plasma temperature and variability with orbital phase suggest that the hard-component emission is caused by a colliding wind shock between the binary components.

Key words: binaries: general – stars: early-type – stars: individual: V444 Cyg – stars: individual: CD Cru – stars: Wolf–Rayet – X-rays: stars.

1 INTRODUCTION

Wolf–Rayet (WR) stars are known to produce strong stellar winds driven by their strong radiation field. The stellar winds can reach velocities up to 1000–3000 km s^{-1} with mass-loss rates of 10^{-4}–10^{-6} M$_\odot$ yr^{-1}, depending upon mass and age (Rauw 2008). These winds not only affect the evolution of the WR stars, but also have a tremendous impact on their surroundings (Rauw 2008). Most O-type and early B-type single stars are reasonably bright ($10^{31} < L_X < 10^{33}$ erg s^{-1}) and are soft ($kT < 1$ keV) X-ray sources. The X-ray luminosity of these sources is found to scale with bolometric luminosity as $L_X/L_{bol} \sim 10^{-7}$ (Berghöfer et al. 1997; Sana et al. 2006). It is generally thought to be produced as a result of shocks, with velocity jumps up to a few hundred km s^{-1}, generated throughout the stellar wind because of dynamic instabilities (Lucy & White 1980; Owocki & Cohen 1999; Kudritzki & Puls 2000). This 'wind-shock' scenario has now become the 'standard' model to explain the X-ray emission from single early-type stars (Rauw 2008, and references therein). However, several massive stars in the Orion Trapezium cluster (Stelzer et al. 2005), the M17 cluster (Broos et al. 2007) and the Carina Nebula (Leutenegger & Kahn 2003) require an additional hard X-ray component to explain their X-ray spectra. This additional hot component is inconsistent with the standard model, which produces only soft X-rays. In order to explain the hard X-ray component, Babel & Montmerle (1997) proposed a magnetically confined wind-shock model. According to this model, the stellar wind is confined by the large-scale magnetic field into the equatorial region. The two streams from the upper and lower hemispheres collide with it to heat the plasma to temperatures much higher than typically expected for single stars from the standard wind-shock model. However, the magnetically confined wind-shock model explains hard X-rays for only a small number of single early-type stars (e.g. θ^1 Ori C; Gagné et al. 2005).

Stellar binary systems with early-type (WR or OB) components are found to be more luminous in X-ray than is expected from the individual components separately (De Becker 2007). This excess X-ray luminosity is thought to originate from the wind–wind interaction zone, where the post-shock temperature is believed to reach up to a few to several tens of million Kelvin (MK), contributing mainly to the harder energy ($kT > 1$ keV) X-ray emissions. The post-shock temperature is expected to be higher in long-period

★E-mail: himali@aries.res.in

(∼ a few weeks) binaries, as the stellar winds collide close to their terminal velocities. In short-period (∼ a few days) binaries, the wind collision occurs while winds are still accelerating (De Becker 2007). However, in both cases, the models predict phase-locked variations in the X-ray domain (Luo, McCray & Mac Low 1990; Usov 1992; Antokhin, Owocki & Brown 2004). These variations are produced either because of the varying circumstellar optical depth along the line of sight towards the shock as the stars revolve around each other or because of a variation in the orbital separation of eccentric binaries, which changes the intrinsic strength of the collision (Nazé et al. 2007; Rauw 2008). In contrast, there are examples of a number of massive star binaries (O+O) that show a weak enhancement in the X-ray emission over single massive stars, but present no variability in the X-ray flux (Albacete Colombo, Méndez & Morrell 2003). Antokhin (2007) has shown that, in general, the X-ray properties of single and binary early-type stars are not very different.

In this paper, we investigate the X-ray emission characteristics for two short-period WR binaries: V444 Cyg and CD Cru. We use high signal-to-noise (S/N) ratio *XMM–Newton* observations. For both objects, the X-ray data from *XMM–Newton* are analysed for the first time; for CD Cru, we analyse the X-ray emission for the first time. Both stars are collected from a systematic study carried out on young galactic clusters using *XMM–Newton* archival data. By choosing these stars associated with young clusters, we obtain good information on the distance and the reddening parameter. Details of the complete study will be presented elsewhere. The relevant parameters of the sample are listed in Table 1, and descriptions of the individual objects are given below.

V444 Cyg (WR 139) is an O6 III–V + WN5 eclipsing binary system associated with the cluster Berkeley 86 (van der Hucht 2001), situated at an estimated distance of 1.9 kpc with $E(B–V) \sim 0.8$ mag (Massey, Johnson & Degioia-Eastwood 1995). The orbital period and the eccentricity of the binary system are estimated to be 4.21 d and 0.03, respectively (Khaliullin, Khaliullina & Cherepashchuk 1984). There are multiwavelength observations of V444 Cyg, and it has well-determined physical parameters. A fairly soft ($kT = 0.5$ keV) thermal X-ray spectrum was reported using observations made with *Einstein* (Moffat et al. 1982). The flux was found to vary by a factor of 2, with a minimum at phase zero, which implies that the WN5 star is in front of the O6 star. Pollock (1987) reported an absorption-corrected flux of $L_X = 7.7 \times 10^{32}$ erg s^{-1} in the 0.4–4 keV range. Using *ROSAT* observations, Corcoran et al. (1996) reported minimum absorption-corrected X-ray luminosities of 3.8×10^{32} erg s^{-1} at the primary eclipse and 8.6×10^{32} erg s^{-1} at the secondary eclipse in the 0.4–4.5 keV range. The *ASCA* observations at three phases in the energy band of 0.7–10 keV were analysed by Maeda et al. (1999). They found the presence of two-temperature (2T; 0.6 and 2.0 keV) plasma, with a soft-component (0.2–4 keV) luminosity of 6–11 $\times$ 10^{32} erg s^{-1}. The high-temperature plasma ($kT \sim 2$ keV) and the variability with the orbital phase suggest that the hard-component emission is caused by shocks originating from the collision of winds from WN5 and O6 stars (Maeda et al. 1999).

CD Cru (WR 47) is an O5 V + WN6 binary system, reported as a member of the cluster Hogg 15 (van der Hucht 2001). Throughout this study, we adopted a distance of 3 kpc for Hogg 15 (see Sagar, Munari & de Boer 2001; Piatti et al. 2002). The orbital period of this binary system is 6.24 d with zero eccentricity (Niemela, Massey & Conti 1980). No previous X-ray observations of the system are reported in the literature.

Our paper is organized as follows. In Sections 2 and 3, we give detailed descriptions of the X-ray data reduction and analysis, respectively. In Section 4, we present a discussion of the X-ray properties of the sources. Finally, we summarize and draw our conclusions in Section 5.

2 X-RAY OBSERVATIONS AND DATA REDUCTION

A log of the X-ray observations is given in Table 2. We made use of archival data obtained with the *XMM–Newton* observatory, which consists of three co-aligned X-ray telescopes observing simultaneously and covering a 30 × 30 arcmin^2 region of the sky. The X-ray

Table 1. Stellar parameters of the WR binaries, V444 Cyg and CD Cru.

Parameters	V444 Cyg	Ref[a]	CD Cru	Ref[a]
Other names	HD 193576; WR 139		HD 311884; WR 47	
Spectral type	O6 III–V + WN5	1	O5 V + WN6	1
Mass ($M_\odot$)	25 + 10	2	57 + 48	10
V (mag)	7.94	3	10.89	11
Distance (pc)	1900	3	3000	12
A_V (mag)	2.48	3	3.56	12
Orbital period (d)	4.21	2	6.24	13
Binary separation ($R_\odot$)	38	2	68	10
Inclination (°)	78	4	70	10
Eccentricity	0.03	5	0	14
$\dot{M}$ (10^{-5} $M_\odot$ yr^{-1})	0.06 + 0.60	6, 4	0.10 + 3.00	15, 10
v_∞ (km s^{-1})	2540 + 1785	7, 8	3000 + 2460	15, 8
log (L_{bol}) erg s^{-1}	39.24 + 38.56	9	39.53 + 38.69	9
Radius ($R_\odot$)	10 + 3	5	57 + 48	10
Cluster membership	Berkeley 86	3	Hogg 15	11

[a] References: 1, van der Hucht et al. (1981); 2, Münch (1950); 3, Massey et al. (1995); 4, Kurosawa, Hillier & Pittard (2002); 5, Cherepashchuk, Eaton & Khaliullin (1984); 6, Marchenko et al. (1997); 7, Underhill & Fahey (1987); 8, Nugis & Lamers (2000); 9, Schaifers & Voigt (1982); 10, Moffat et al. (1990); 11, Moffat (1974); 12, Sagar et al. (2001); 13, Niemela et al. (1980); 14, Cherepashchuk & Karetnikov (2003); 15, Repolust, Puls & Herrero (2004) (typical value for the spectral type).

Table 2. Journal of *XMM–Newton* observations of the objects in the sample.

Object name	Observation ID	Exposure time (s)	Start time UT (hh:mm:ss)	EPIC filter	Offset from target (arcmin)	Orbital phase
V444 Cyg	0206240201	10032	2004 May 19 12:35:42	Thick	0.001	0.13 (0.12–0.14)
	0206240301	11914	2004 May 27 12:01:39	Thick	1.120	0.03 (0.01–0.04)
	0206240401	11915	2004 May 29 12:01:49	Thick	1.162	0.51 (0.50–0.51)
	0206240501	11918	2004 Jun 06 11:36:30	Thick	1.111	0.39 (0.38–0.41)
	0206240701	11911	2004 Jun 14 10:58:29	Thick	1.133	0.29 (0.27–0.30)
	0206240801	19921	2004 Oct 27 23:47:44	Thick	1.093	0.47 (0.45–0.50)
CD Cru	0109480101	53046	2002 Jul 03 15:51:56	Thick	2.812	0.78 (0.73–0.83)
	0109480201	48015	2002 Aug 26 21:55:14	Thick	3.848	0.47 (0.43–0.51)
	0109480401	53040	2003 Jan 21 01:07:38	Thick	4.969	0.05 (0.01–0.09)

photons were recorded with the European Photon Imaging Camera (EPIC), which forms images on three CCD-based detectors: the PN (Strüder et al. 2001) and the twin MOS1 and MOS2 (Turner et al. 2001) with an angular resolution of 6 arcsec (FWHM). During the observations, all three EPIC detectors were active in full-frame mode together with the thick filter. For V444 Cyg, six separate observations were taken with the exposure time ranging from 10 to 20 ks. These observations are spread over the half-cycle of the binary system. However, for CD Cru, three separate observations were taken, covering almost the full binary cycle.

2.1 EPIC data reduction

We reduced the X-ray data using standard *XMM–Newton* Science Analysis System software (SAS version 7.0.0) with updated calibration files (Ehle et al. 2004). The event files for the MOS and PN detectors were generated using the tasks EMCHAIN and EPCHAIN, respectively. These tasks allow the calibration of the energy and the astrometry of the events registered in each CCD chip, and allow us to combine these in a single data file. We restricted our analysis to the energy band 0.3–7.5 keV, as data below 0.3 keV are mostly unrelated to bona fide X-rays, and data above 7.5 keV are mostly dominated by background counts. The event list files were extracted using the SAS task EVSELECT. Data from the three cameras were individually screened for the time intervals with high background when the total count rates (for single events of energy above 10 keV) in the instruments exceeded 0.35 and 1.0 counts s^{-1} for the MOS and PN detectors, respectively. The observations with observation ID 0206240401 for the source V444 Cyg were heavily affected by high background events, and the data in the MOS detectors were not useful. Only half of the observation time ($\sim$5 ks) with PN was found to be useful.

The light curves and spectra were extracted using a circular region with the source as the centre in the energy range 0.3–7.5 keV of the EPIC detectors. The X-ray sources in the cluster were often found to be largely contaminated because of emission from the neighbouring sources. For this reason, the radii of the extraction regions were varied between 20 and 30 arcsec, depending upon the position of the sources in the detector and their angular separation between the neighbouring X-ray sources. The background has been estimated from a number of empty regions close to the X-ray source in the same CCD of the detector. The X-ray spectra of the sources were generated using the SAS task ESPECGET, which also computes the photon redistribution as well as the ancillary matrix. For each source, the background spectrum was obtained from regions devoid of any sources chosen according to the source location. Finally, the spectra were re-binned to have at least 20 counts per spectral bin for both sources in all the observations.

2.2 Reflection grating spectrometer data reduction

The reflection grating spectrometers (RGS) are mounted on two of the three *XMM–Newton* X-ray telescopes. They were operated in spectroscopy mode during the observations. We followed the standard procedure as outlined in the *XMM–Newton* handbook to generate the RGS spectra of the sources. The raw data were processed with the task RGSPROC at the position of the sources. The other bright sources, found in the same field observed by the RGS, have been excluded from the background estimation. In addition, we have filtered the event list for high background level events. For V444 Cyg, the data obtained for observations with observation ID 0206240401 were contaminated with high background events in the RGS detector, and therefore the data are not useful. For CD Cru, the two observations ID 0109480101 and 0109480201 were not useful as they were heavily contaminated by a brighter source, HD 110432, and affected by high background episodes, respectively.

3 ANALYSIS AND RESULTS

3.1 X-ray light curves

The background-subtracted X-ray light curves of the WR binaries, V444 Cyg and CD Cru, as observed with the PN detector, are shown in Figs 1(a) and (b), respectively. The light curves in the 0.3–7.5 keV (total) energy band show the variability, which suggests colliding wind shocks. We also performed a χ^2 test to measure the significance of the deviations from the mean count rate, in order to quantify the constancy of the data over the timescale of observations. We found the variability in the light curves to have a confidence level greater than 99.999 per cent for both binaries. In order to investigate the variability in the different energy bands, the light curves of these binaries obtained with the MOS and PN data are generated into two energy bands: soft (0.3–2.0 keV) and hard (2.0–7.5 keV). The hardness ratio (HR) is defined by the ratio of hard to soft band count rates. The total, hard and soft band intensity curves, and the HR curve as a function of the orbital phase, are shown in the panels running from top to bottom in Figs 2a (PN) and 2b (MOS) for the WR binary V444 Cyg. Similar plots of intensity and HR for CD Cru are shown in Fig. 3. The phases of the observations are calculated using the ephemeris HJD = 244 1164.337 + 4.213E for V444 Cyg (Underhill, Grieve & Louth 1990) and HJD = 244 3918.4000 + 6.2399E for CD Cru (Niemela et al. 1980; Moffat et al. 1990). Here, the phase 0.0 indicates the

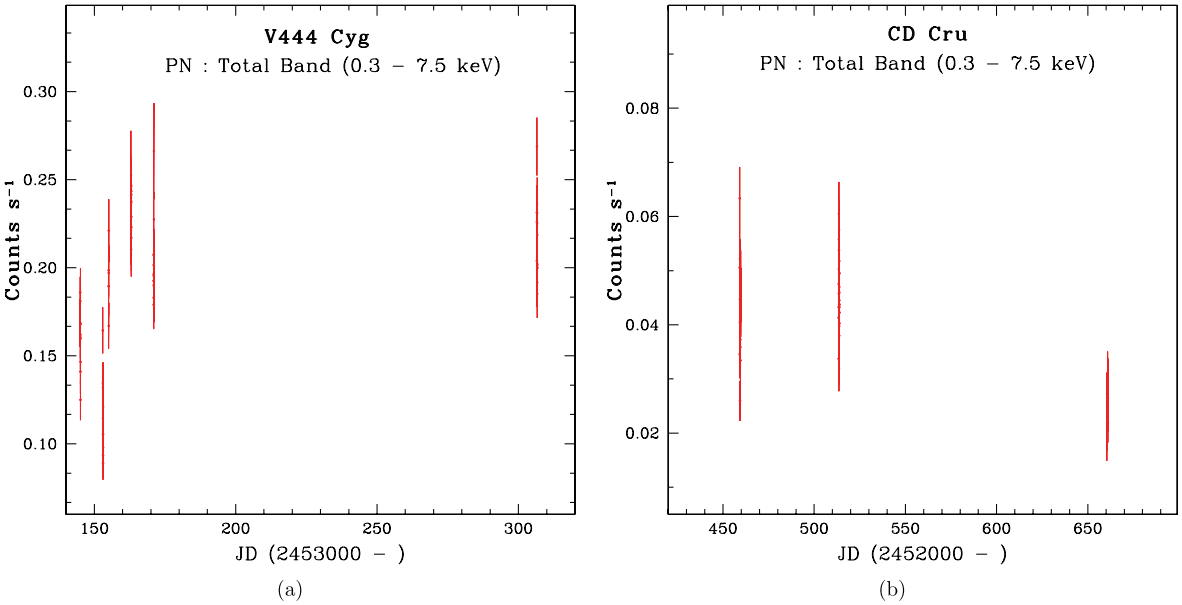

Figure 1. X-ray light curves of the WR binaries (a) V444 Cyg and (b) CD Cru in the 0.3–7.5 keV energy band.

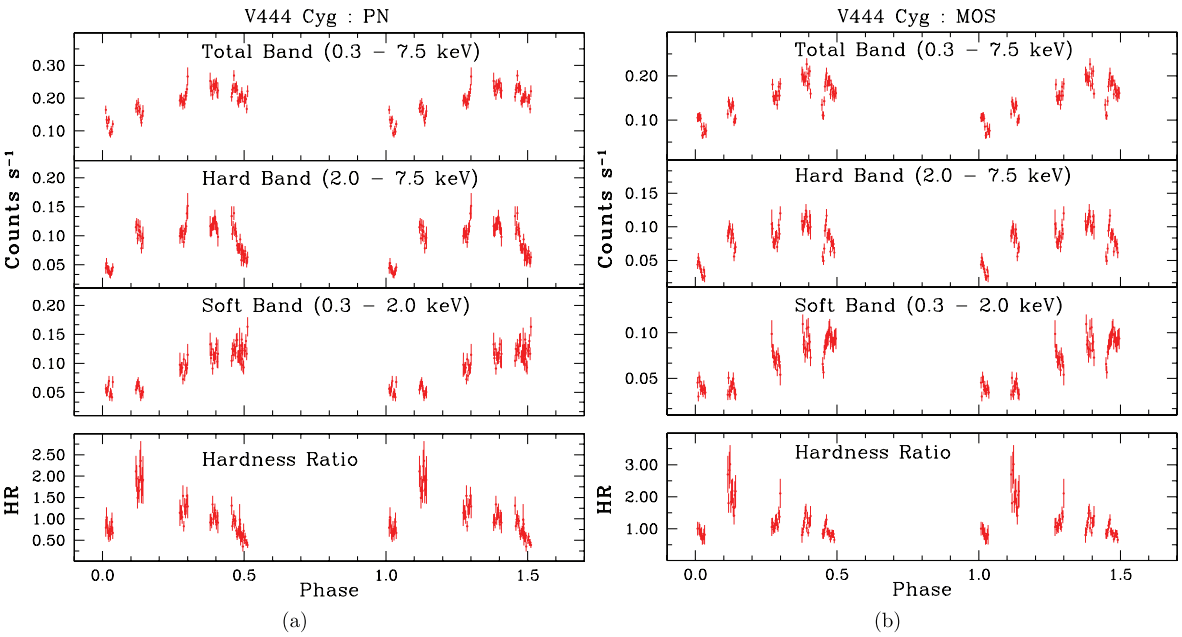

Figure 2. (a) PN and (b) MOS light curves at three energy bands, total (0.3–7.5 keV), soft (0.3–2.0 keV) and hard (2.0–7.5 keV), and the HR curve as a function of orbital phase, where HR = hard/soft of V444 Cyg.

primary eclipse and the phase 0.5 indicates the secondary eclipse. The light curves in the individual bands show the phase-locked variability for both binaries. For V444 Cyg, the count rates in the total energy band were minimum at phase 0.0 and maximum at phase 0.45. After phase 0.45, the count rates were decreased up to phase 0.5. The count rates are increased by a factor of ∼2, being minimum at phase 0.0 in the total energy band. In the soft band, the count rates were minimum at phase 0.0 and maximum during the phase 0.45–0.5. However, in the hard-band light curve, two minima at phases 0.0 and 0.5 were seen clearly. During the phases from 0.13 to 0.45 (i.e. outside the eclipse), the count rates in the hard band were constant. The HR curve can reveal information about the spectral variations. The HR curve shows that the emitted X-ray is harder just after phase 0.0, being maximum at phase 0.13, and afterward decreases until phase 0.5. In the case of CD Cru, the nature of the variability was found to be similar to that seen in V444 Cyg. In the soft band, the count rates were found to be constant during phases 0.47 and 0.78 (i.e. outside the eclipse). However, the count rates decrease rapidly after phase 0.47 in the hard band. A small variation was also observed in the HR curve of CD Cru. It was maximum at phase 0.0 and minimum during phase 0.47.

3.2 X-ray spectra and spectral fits

The EPIC spectra of WR binaries in different phases are shown in Figs 4 and 5 for V444 Cyg and CD Cru, respectively. Below

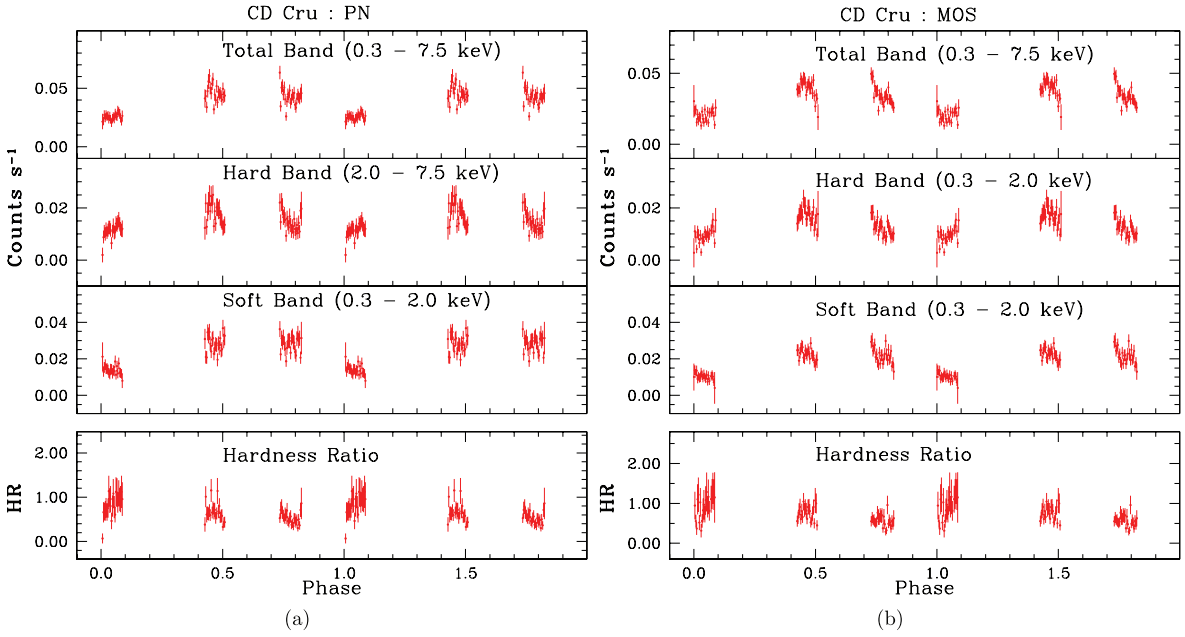

Figure 3. Same as Fig. 2 but for CD Cru.

1 keV, the spectra were found to be affected by the high extinction, as previously observed with *ASCA* for V444 Cyg (Maeda et al. 1999). Strong emission lines are seen in the MOS and PN spectra of both WR binaries. The most prominent lines found in the spectra (along with their laboratory energies) are the following: Fe XVII (0.8 keV), Ne X (1.02 keV), Mg XII (1.47 keV), Si XIII (1.853 keV), S XV (2.45 keV), Ar XVII (3.12 keV), Ca XIX+XX (3.9 keV) and Fe XXV (6.63 keV).

In order to trace the spectral parameters at different binary phases, we performed spectral analysis of each data set using simultaneous fitting of EPIC data by two models: (i) plane-parallel shock model (VPSHOCK; Borkowski, Lyerly & Reynolds 2001); (ii) models of the Astrophysical Plasma Emission Code (APEC; Smith et al. 2001), as implemented in XSPEC version 12.3.0. A χ^2 minimization gave the best fitted model to the data. The presence of interstellar material along the line of sight and the local circumstellar material around the stars can modify the X-ray emission from massive stars. We corrected for the local absorption in the line of sight to the source using photoelectric absorption cross-sections according to Balucińska-Church & McCammon (1992) and modelled as PHABS (photoelectric absorption screens) with two absorption components, $N_{\rm H}^{\rm ISM}$ and $N_{\rm H}^{\rm local}$. $N_{\rm H}^{\rm ISM}$ was estimated using the relation, $N_{\rm H} = 5.0 \times 10^{21} \times E(B–V)$ cm^{-2} (Vuong et al. 2003), where $E(B–V) = A_{\rm V}/3.1$, assuming a normal interstellar reddening law towards the direction of the cluster. We used values of $A_{\rm V}$ of nearly 2.48 and 3.56 mag derived for clusters Berkeley 86 (Massey et al. 1995) and Hogg 15 (Sagar et al. 2001), respectively. The estimated values of $N_{\rm H}^{\rm ISM}$ towards V444 Cyg and CD Cru are found to be 4.0×10^{21} and 6.0×10^{21} cm^{-2}, respectively. $N_{\rm H}^{\rm local}$ was estimated by making a fit to the observed spectra by varying the local environment for the soft (kT_1) and hard (kT_2) energy components in terms of $N_{\rm H}^1$ and $N_{\rm H}^2$, respectively. Because WN stars are at evolved stages, the abundances of He, C, N, O, Ne, Mg, Si, S, Ar, Ca and Fe were allowed to vary during the fitting procedure to account for the observed line emission. The solar abundances were adopted from Lodders (2003).

First, we fitted the VPSHOCK plasma model to derive the spectral features. The constant temperature VPSHOCK plasma model was considered without incorporating the mass-loss and orbital parameters of WR stars. However, the model does account for non-equilibrium ionization effects and assumes an equal electron and ion temperature. The best-fitting VPSHOCK models to the data for the WR stars are given in Tables 3 and 4 for V444 Cyg and CD Cru, respectively.

X-ray emitting plasma may not be isothermal and the observed X-ray spectrum may be a superposition of a cool stellar component and a hot colliding wind shock plasma, as a number of emission lines in the spectra can be formed over a range of temperatures. The cooler component is believed to arise from the instabilities in radiation-driven outflows. However, using the X-ray imaging data of *XMM–Newton* it is not possible to resolve the X-ray emission from the colliding wind region and individual stars separately. Therefore, secondly, we fitted the 2T plasma model 'VAPEC' to characterize such components. The form of 2T plasma model was PHABS(PHABS*VAPEC+PHABS*VAPEC). In terms of χ^2, the 2T plasma model provides better goodness of fit for both sources over the VPSHOCK model. The results for the 2T plasma model along with the data are displayed in Figs 4 and 5 for V444 Cyg and CD Cru, respectively. The best-fitting parameters are given in Tables 3 and 4 for V444 Cyg and CD Cru, respectively.

3.3 Evolution of spectral parameters

The spectral analysis at different phases of the WR binaries provides the dependence of the best-fitting values of parameters in the orbital phase. Figs 6(a) and 6(b) show the variation of the soft-band ($L_{\rm X}^{\rm S}$) and hard-band ($L_{\rm X}^{\rm H}$) X-ray luminosities, the column densities corresponding to the cool ($N_{\rm H}^1$) and hot ($N_{\rm H}^2$) temperature components and the cool(kT_1) and hot (kT_2) temperatures as a function of the orbital phases for V444 Cyg and CD Cru, respectively. For V444 Cyg, $L_{\rm X}^{\rm H}$ was found to be minimum during the primary and secondary eclipses and maximum outside the eclipse. It was constant during phase 0.13–0.47. However, $L_{\rm X}^{\rm S}$ was found to be minimum during the primary eclipse only. At phase 0.5, $L_{\rm X}^{\rm S}$ was found to be maximum. Both $L_{\rm X}^{\rm H}$ and $L_{\rm X}^{\rm S}$ were found to be minimum during phase 0.0 and maximum at phase 0.5 for the WR binary CD Cru. The

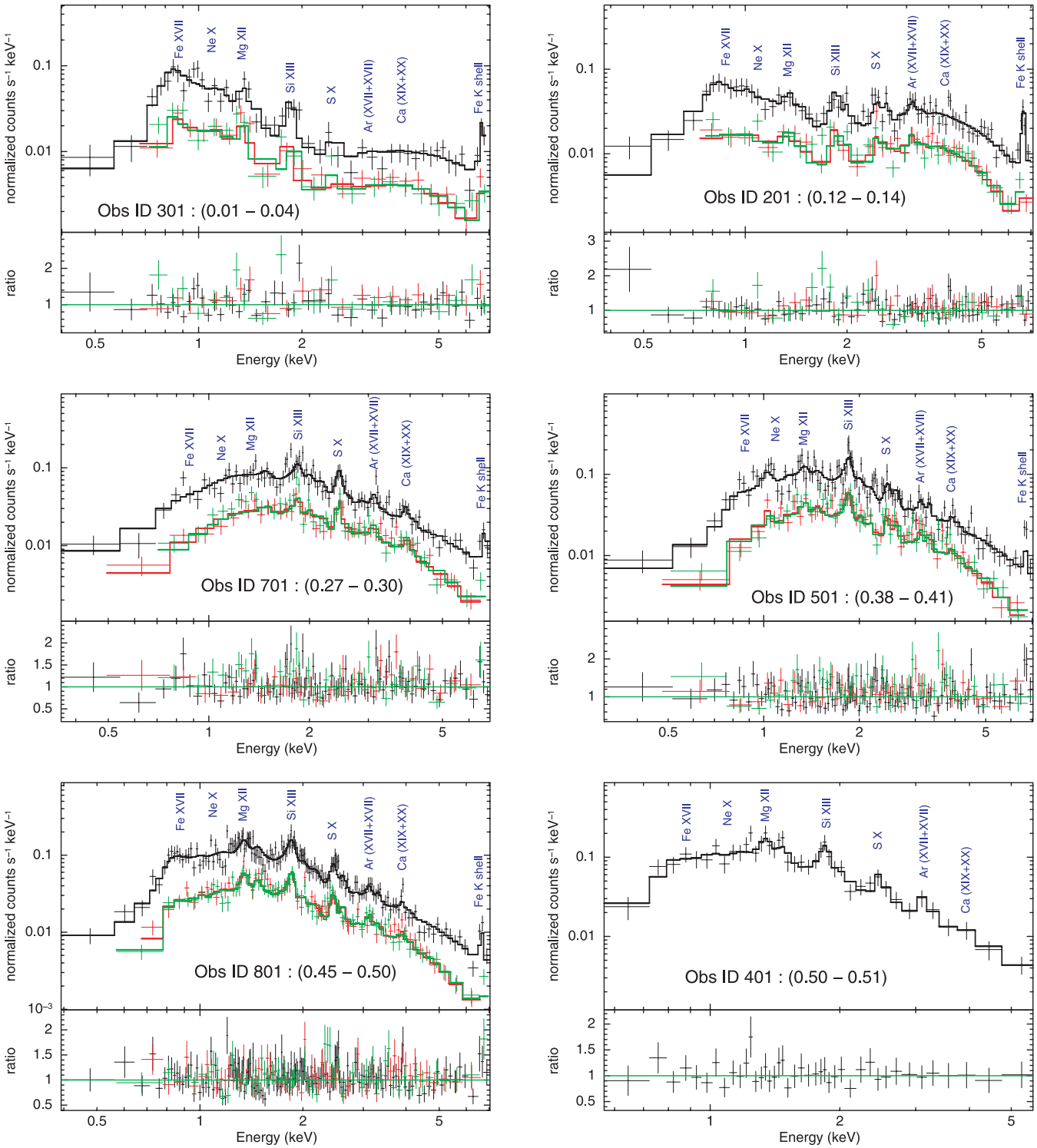

Figure 4. X-ray spectra of MOS and PN data with the best-fitting 2T VAPEC model in the upper subpanels of each graph for V444 Cyg. The χ^2 distributions in terms of ratio are given in the lower subpanels of each graph. The last three digits of the observation ID and the corresponding phases of the observations are given in each graph.

cool component (kT_1) was found to be constant with a mean value of 0.61 ± 0.05 and 0.57 ± 0.10 keV for V444 Cyg and CD Cru, respectively. The hard energy component (kT_2) was varied from a minimum value of 1.88 keV to a maximum value of 9.61 keV for V444 Cyg. It was maximum at the primary eclipse and at phase 0.29, and minimum during the secondary eclipse and at phase 0.13. For CD Cru, kT_2 varies from a minimum value of 1.63 keV outside the eclipse to a maximum value of 4.27 keV at the primary eclipse. For V444 Cyg, $N_{\rm H}^1$ was maximum at phase 0.29, and otherwise it was constant at all phases. However, $N_{\rm H}^1$ was found to be constant throughout the orbital phase with a mean value of 1.14 ± 0.11 × 10^{22} cm^{-2} for CD Cru. For V444 Cyg, $N_{\rm H}^2$ was increased from

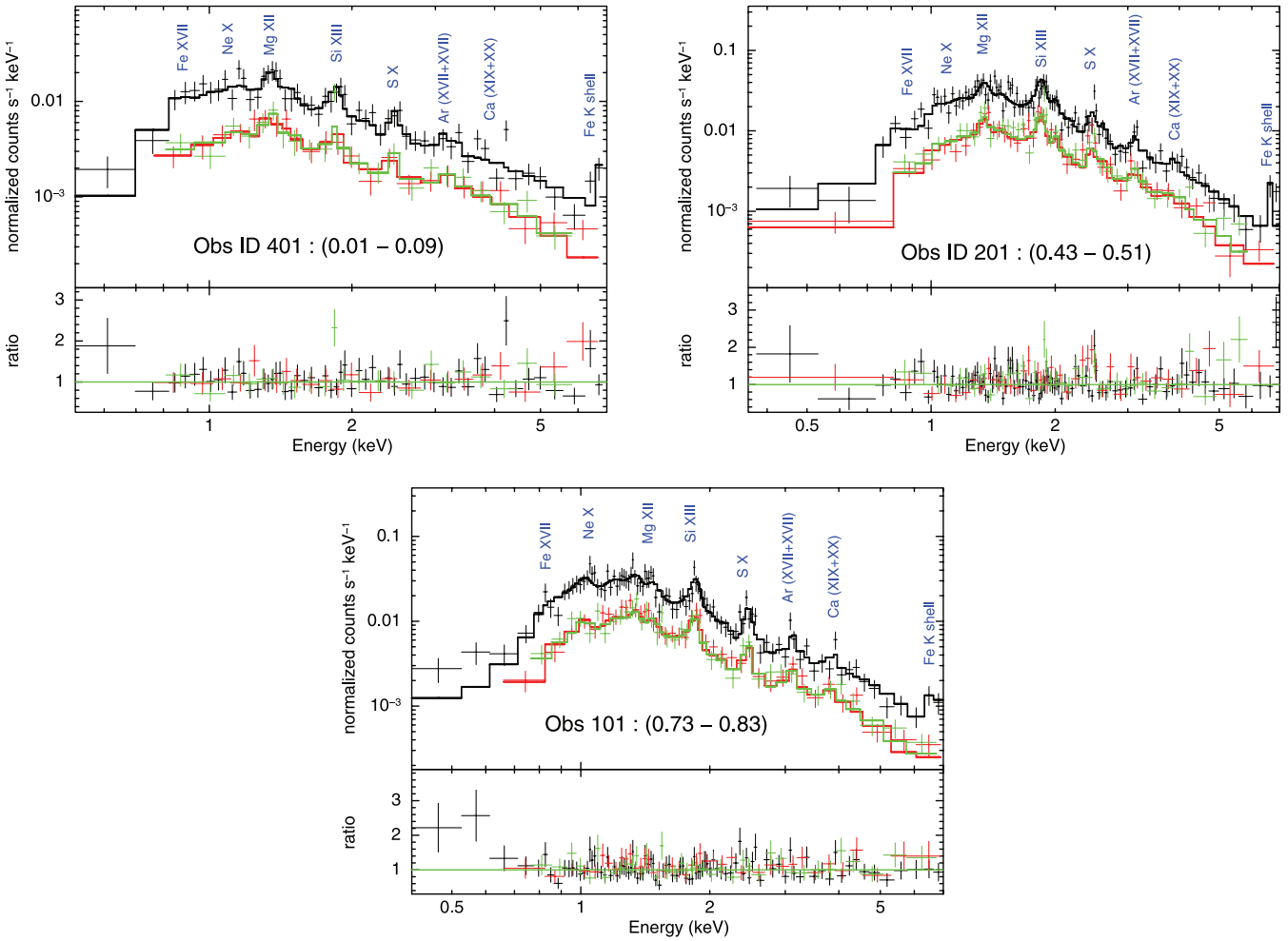

Figure 5. Same as Fig. 4 but for CD Cru.

phase 0.0 to its maximum value at phase 0.13. Afterwards, it was decreased and became almost constant from phase 0.29 to phase 0.47. For CD Cru, $N_{\rm H}^2$ was minimum at phase 0.0 and maximum at phase 0.78.

3.4 RGS spectra

We combined the first- and second-order spectra of detectors RGS1 and RGS2 to inspect the main spectral lines. We obtained the RGS fluxed spectra using task RGSFLUXER, which is shown in Fig. 7 for different phases for both binaries. We identified the prominent emission lines for V444 Cyg at wavelengths Mg XII (6.50 Å; 6.74 Å), Mg XI (9.23 Å), Fe XVIII (11.40 Å) and Ca XVI (22.61 Å, 21.43 Å, 22.30 Å). Individual lines show intensity variations from spectrum to spectrum. Unfortunately, our observations are at the limit of detectability with the data available with poor count statistics. Therefore, the S/N ratios of individual lines are not sufficient to perform a detailed quantitative analysis of the RGS line spectrum for any of the massive stars.

4 DISCUSSION

We have analysed the X-ray emission properties of two WR binaries with strong stellar winds. Below, we discuss the implications of the X-ray results.

4.1 Phase-locked X-ray variability

The X-ray temporal and spectral analyses of WR binaries V444 Cyg and CD Cru show a phase-locked phenomenon. The phase-resolved X-ray spectroscopic observations show that the soft energy component and the corresponding $N_{\rm H}^1$ were also found to be nearly constant throughout the binary phases of both stars. $L_{\rm X}^{\rm S}$ was found to be minimum during the primary eclipse only. These results lead to the radiative wind shock origin of the soft energy component. For CD Cru, the modulation of $L_{\rm X}^{\rm S}$ matches well with the optical light curve reported by Moffat et al. (1990). Lamontagne et al. (1996) have reported a similar shape of optical photometric light curves for 13 WR binaries, including CD Cru, and have said that it could be a result of the 'atmospheric eclipse'. The X-ray flux in the hard energy band was found to be minimum at both primary and secondary eclipses for both stars. This implies that the hard energy component could be a result of the presence of the wind–wind collision zone, which is located somewhere in between the O-type and WR star, and is therefore minimum when either of the stars in the binary system is eclipsed. A similar behaviour of X-ray light curves was seen in the *Einstein*, *ROSAT* and *ASCA* observations of V444 Cyg (Moffat et al. 1982; Corcoran et al. 1996; Maeda et al. 1999). The hot temperature (kT_2) and the corresponding $N_{\rm H}^2$ were also varied with the orbital phases of both binaries. The eccentricity of both binary systems is almost zero, and therefore

Table 3. Spectral parameters derived from the best-fitting VPSHOCK model and the 2T VAPEC plasma models for V444 Cyg. Here, $\chi^2_\nu = \chi^2/\nu$, where ν is degrees of freedom. Errors are with 90 per cent confidence based on $\chi^2_{\rm min} + 2.71$. $N^1_{\rm H}$ and $N^2_{\rm H}$ are in units of 10^{22} cm^{-2} . kT_1 and kT_2 are in units of keV. τ is in units of 10^{11} s cm^{-3} . EM_1 and EM_2 are in units of 10^{54} cm^{-3} . $L^{\rm T}_{\rm X}$ luminosity in band 0.3–7.5 keV, $L^{\rm S}_{\rm X}$ luminosity in band 0.3–2.0 keV and $L^{\rm H}_{\rm X}$ luminosity in band 2.0–7.5 keV are in units of erg s^{-1}.

	V444 Cyg											
	Obs ID: 0206240201 Phase: 0.12–0.14		Obs ID: 0206240301 Phase: 0.01–0.04		Obs ID: 0206240401 Phase: 0.50–0.51		Obs ID: 0206240501 Phase: 0.38–0.41		Obs ID: 0206240701 Phase: 0.27–0.30		Obs ID: 0206240801 Phase: 0.45–0.50	
	VPSHOCK	2T VAPEC	VPSHOCK	2T VAPEC	VPSHOCK	2T VAPEC	VPSHOCK	2T VAPEC	VPSHOCK	2T VAPEC	VPSHOCK	2T VAPEC
$N^1_{\rm H}$	0.75	$0.48^{+0.20}_{-0.12}$	0.280	$0.64^{+0.16}_{-0.24}$	$0.17^{+1.46}_{-0.18}$	$0.47^{+0.26}_{-0.68}$	$1.46^{+0.30}_{-0.18}$	$0.85^{+0.20}_{-0.25}$	$1.71^{+0.15}_{-0.40}$	$8.40^{+3.42}_{-2.88}$	$0.43^{+0.15}_{-0.19}$	$0.78^{+0.12}_{-0.11}$
$N^2_{\rm H}$		$11.86^{+1.66}_{-1.88}$		$9.35^{+4.23}_{-2.50}$		<12.20		$2.74^{+1.71}_{-0.91}$		<0.17		$2.33^{+0.76}_{-0.84}$
kT_1	79.80	$0.57^{+0.07}_{-0.13}$	79.90	$0.60^{+0.04}_{-0.04}$	$2.33^{+0.74}_{-0.48}$	$0.62^{+0.12}_{-0.13}$	$3.14^{+0.92}_{-0.43}$	$0.58^{+0.09}_{-0.10}$	$3.48^{+0.55}_{-0.46}$	$0.70^{+0.15}_{-0.10}$	$4.21^{+0.70}_{-0.78}$	$0.60^{+0.03}_{-0.03}$
kT_2		$1.85^{+0.22}_{-0.26}$		$8.16^{+5.35}_{-4.16}$		$1.97^{+5.70}_{-0.95}$		$3.64^{+1.01}_{-0.97}$		$9.61^{+3.51}_{-1.97}$		$3.22^{+0.68}_{-0.34}$
τ	0.23		0.18		$0.38^{+0.82}_{-0.19}$		$0.73^{+0.23}_{-0.20}$		$0.58^{+0.18}_{-0.14}$		$0.35^{+0.10}_{-0.07}$	
EM_1	0.19	<5.32	0.17	<22.54	<4.25	<288.07	$1.72^{+0.65}_{-0.80}$	$29.33^{+60.06}_{-7.17}$	<35.92	$3.51^{+20.73}_{-2.52}$	<11.77	$30.32^{+50.70}_{-22.53}$
EM_2		$5.10^{+0.72}_{-0.81}$		$13.60^{+122.46}_{-6.11}$		<36.44		<74.03		<25.367		$16.28^{+48.01}_{-12.86}$
He	763.00	<30.15	518.90	<0.14	<9997.63	≈0.00	<951.62	<728.99	$617.61^{+9380.65}_{-201.57}$	>40.18	$9973.5^{+9520.95}_{-199.229}$	>20.04
C	9998.91	<693.28	0.00	≈0.00	≈0.00	≈0.00	≈0.00	<258.19	≈0.00	≈0.00	<9999.97	<109.71
N	650.45	<651.73	0.00	≈0.00	<9998.63	≈0.00	≈0.00	≈0.00	>400.059	≈0.00	<98.928	<885.30
O	191.35	$377.38^{+50.80}_{-33.99}$	2.13	<66.17	<25.84	≈0.00	$1114.90^{+9667.15}_{-201.29}$	<191.51	$3054.69^{+7682.71}_{-48.20}$	<316.85	<37.34	<18.09
Ne	68.34	<80.79	33.83	<20.27	<11.42	<150.67	<58.76	$10.13^{+64.95}_{-3.96}$	<61.40	<446.78	<2.96	<0.49
Mg	0.00	$31.77^{+130.88}_{-26.32}$	76.34	$38.42^{+365.20}_{-7.61}$	$40.46^{+289.49}_{-17.30}$	$29.21^{+225.47}_{-10.36}$	$5.34^{+9.53}_{-4.66}$	$2.83^{+15.40}_{-2.13}$	<46.27	<658.42	$13.17^{+6.66}_{-4.49}$	$1.43^{+2.98}_{-0.62}$
Si	0.00	$62.63^{+152.45}_{-40.66}$	142.88	$37.36^{+344.36}_{-9.20}$	$78.56^{+454.70}_{-35.98}$	$97.03^{+220.92}_{-13.96}$	$21.20^{+56.08}_{-3.95}$	$3.19^{+80.86}_{-5.29}$	$73.63^{+37.30}_{-24.93}$	$120.13^{+411.08}_{-68.09}$	$47.98^{+16.25}_{-9.83}$	$4.59^{+33.75}_{-1.00}$
S	999.97	$38.33^{+135.50}_{-17.19}$	199.06	$73.74^{+664.80}_{-19.03}$	$217.19^{+460.11}_{-133.78}$	$58.63^{+491.05}_{-19.90}$	$25.91^{+85.94}_{-8.20}$	<72.61	$212.54^{+109.78}_{-33.55}$	$203.53^{+250.52}_{-91.46}$	$184.70^{+855.09}_{-40.00}$	$44.18^{+38.89}_{-3.08}$
Ar	6.02	<119.86	6.02	<64.00	≈0.00	>2.77	≈0.00	$28.83^{+32.02}_{-16.22}$	≈0.00	$246.82^{+380.31}_{-194.31}$	≈0.0	$23.98^{+67.11}_{-3.75}$
Ca	9991.50	<11.46	2994.71	<97.37	<995.93	<337.62	$89.45^{+125.95}_{-70.88}$	<37.60	$631.16^{+9999.82}_{-260.60}$	>182.96	<9997.92	$4.89^{+35.39}_{-4.28}$
Fe	92.50	$20.95^{+101.17}_{-24.64}$	196.91	$66.99^{+620.40}_{-7.20}$	$14.27^{+113.12}_{-9.40}$	$9.22^{+157.32}_{-8.12}$	$23.31^{+105.67}_{-13.01}$	$1.93^{+12.98}_{-1.45}$	$162.51^{+9836.23}_{-106.27}$	$142.33^{+124.11}_{-57.97}$	$11.35^{+7.76}_{-7.19}$	$1.11^{+4.37}_{-0.31}$
χ^2_ν (d.o.f.)	2.77(130)	1.07 (127)	2.38(79)	1.28 (77)	1.10 (27)	0.77 (25)	1.47 (200)	1.38 (198)	1.13 (168)	1.08 (166)	1.12(277)	0.98 (275)
L^T_X		32.691		32.485		32.589		32.764		32.726		32.732
L^S_X		31.739		31.746		32.170		32.104		31.999		32.177
L^H_X		32.639		32.398		32.380		32.657		32.636		32.591

Table 4. Spectral parameters derived from the best-fitting VPSHOCK model and 2T VAPEC plasma models for CD Cru. The units of the parameters are the same as those given in Table 3. Here, $\chi^2_\nu = \chi^2/\nu$, where ν is degrees of freedom. Errors are with 90 per cent confidence based on $\chi^2_{\rm min} + 2.71$.

	CD Cru					
	Obs ID: 0109480101 Phase: 0.73–0.83		Obs ID: 0109480201 Phase: 0.43–0.51		Obs ID: 0109480401 Phase: 0.01–0.09	
	VPSHOCK	2T VAPEC	VPSHOCK	2T VAPEC	VPSHOCK	2T VAPEC
$N_{\rm H}^1$	$1.44^{+0.14}_{-0.22}$	$1.07^{+0.20}_{-0.29}$	$0.27^{+0.12}_{-0.10}$	$1.27^{+0.21}_{-0.09}$	$0.78^{+0.19}_{-0.16}$	$1.08^{+0.20}_{-0.26}$
$N_{\rm H}^2$		<19.57		$4.49^{+1.57}_{-1.75}$		$3.88^{+2.64}_{-1.96}$
kT_1	$2.67^{+0.82}_{-0.82}$	$0.65^{+0.13}_{-0.04}$	$3.02^{+0.51}_{-0.42}$	$0.46^{+0.14}_{-0.14}$	$7.69^{+7.08}_{-3.05}$	$0.59^{+0.05}_{-0.07}$
kT_2		$1.63^{+2.26}_{-0.23}$		$1.81^{+0.31}_{-0.29}$		$4.27^{+4.81}_{-2.39}$
τ	$0.60^{+0.12}_{-0.13}$		$1.19^{+0.51}_{-0.35}$		$0.25^{+0.07}_{-0.05}$	
EM_1	$>8.80 \times 10^4$	$0.55^{+25.35}_{-0.17}$	$0.03^{+0.62}_{-0.01}$	$6.33^{+57.90}_{-0.30}$	<0.44	<270.41
EM_2		<45.06		$0.82^{+0.49}_{-0.44}$		<45.68
He	$493.48^{+9492.43}_{-421.12}$	<202.72	$5319.53^{+7609.94}_{-29.35}$	<171.03	$375.17^{+9580.50}_{-145.95}$	≈0.00
C	<9999.98	≈0.00	≈0.00	<445.56	≈0.00	≈0.00
N	≈0.0	≈0.00	< 9999.53	<805.06	≈0.00	≈0.00
O	$4947.23^{+7632.81}_{-5.07}$	>137.01	< 100.83	>137.33	< 421.57	≈0.00
Ne	<195.20	$217.83^{+122.88}_{-107.12}$	< 200.47	$82.73^{+103.68}_{-65.56}$	< 45.27	<3.95
Mg	$110.50^{+52.64}_{-26.30}$	$84.33^{+33.16}_{-37.95}$	$312.97^{+133.48}_{-105.30}$	$79.94^{+58.32}_{-32.51}$	$64.24^{+115.36}_{-20.92}$	$27.17^{+29.04}_{-0.64}$
Si	$256.53^{+52.64}_{-52.64}$	$101.23^{+54.24}_{-31.93}$	$801.39^{+8604.51}_{-263.32}$	$163.73^{+92.97}_{-75.87}$	$80.84^{+89.41}_{-33.29}$	$6.46^{+29.71}_{-0.27}$
S	$298.46^{+105.28}_{-52.64}$	$191.89^{+81.16}_{-69.29}$	$1090.01^{+438.26}_{-172.37}$	$125.29^{+81.78}_{-40.03}$	$193.76^{+277.87}_{-84.88}$	$21.85^{+207.92}_{-1.64}$
Ar	≈0.0	<73.88	≈0.00	$101.34^{+120.36}_{-73.27}$	≈0.00	>1.32
Ca	>862.33	<318.32	<3889.83	<262.68	<948.97	<5.50
Fe	$780.96^{+210.56}_{-421.12}$	$90.78^{+81.92}_{-78.33}$	<237.873	$86.23^{+79.64}_{-38.00}$	$104.73^{+202.96}_{-58.14}$	$5.38^{+50.63}_{-1.07}$
χ^2_ν (d.o.f.)	1.06(164)	1.01 (162)	1.44(173)	1.32 (171)	0.98(89)	0.95 (87)
$F_{\rm X}$	0.23	0.23	0.26	0.26	0.19	0.19
$L_{\rm X}^{\rm T}$		32.391		32.451		32.309
$L_{\rm X}^{\rm S}$		31.941		31.959		31.687
$L_{\rm X}^{\rm H}$		32.200		32.282		32.190

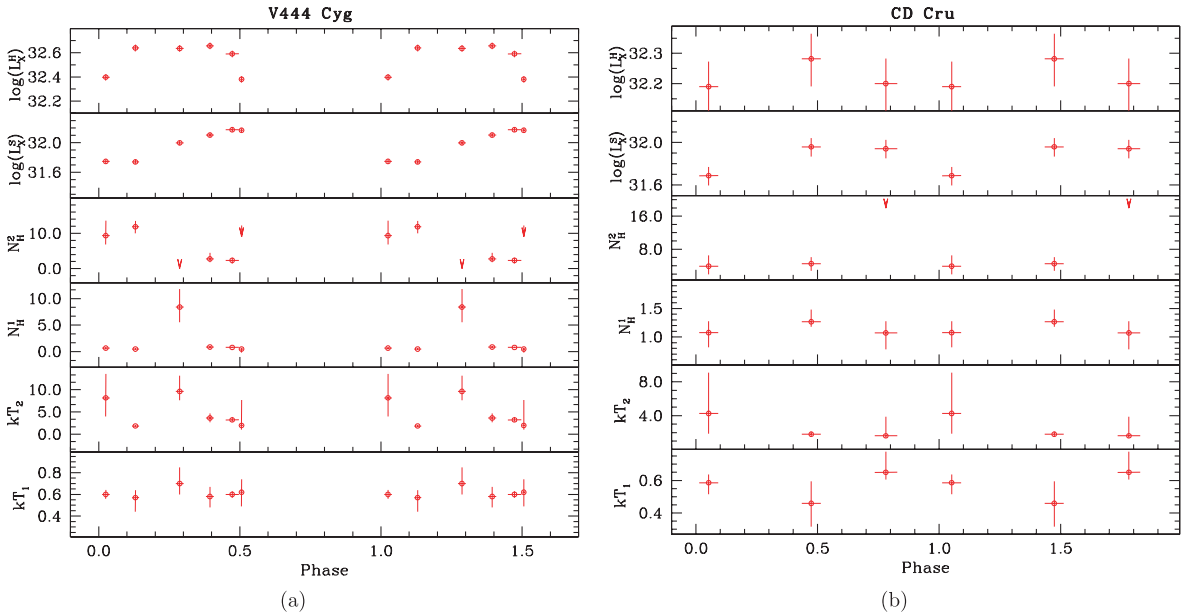

Figure 6. Variation of $L_{\rm X}^{\rm S}$, $L_{\rm X}^{\rm H}$, $N_{\rm H}^1$, $N_{\rm H}^2$, kT_1 and kT_2 as a function of the orbital phases of (a) V444 Cyg and (b) CD Cru.

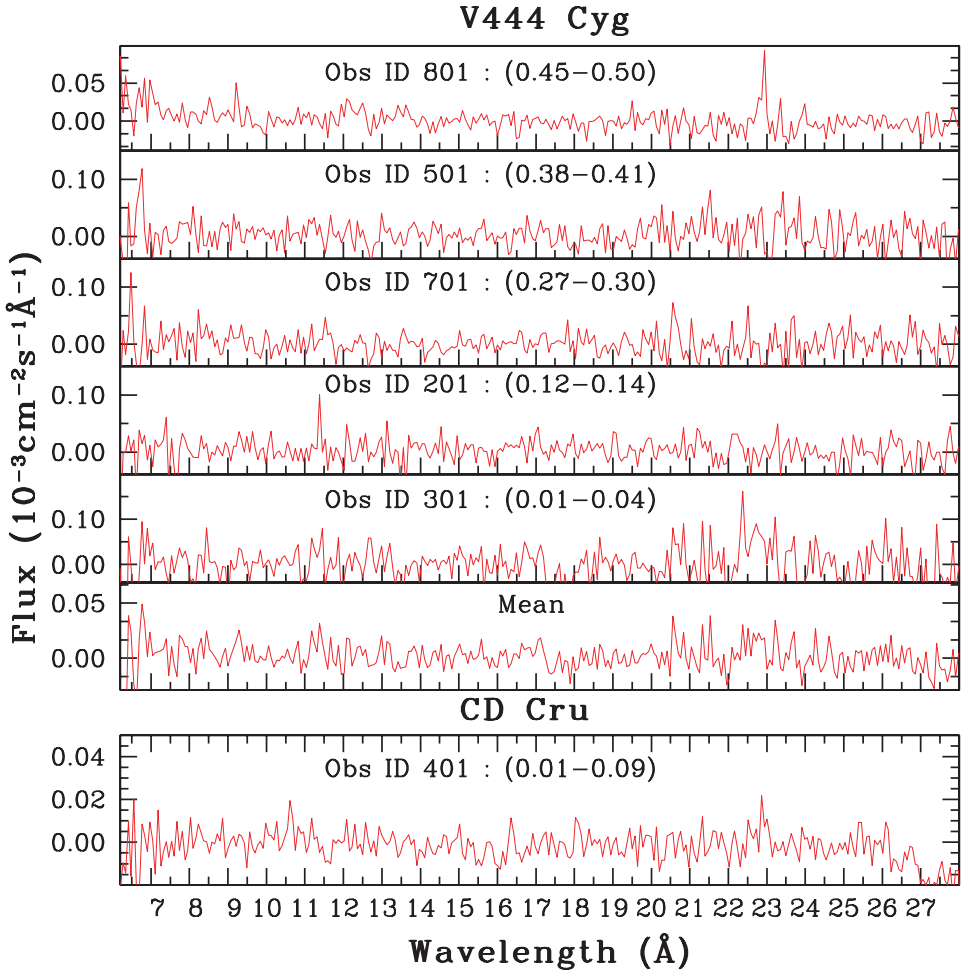

Figure 7. RGS spectra of the WR binaries at different binary phases for V444 Cyg (upper panel) and CD Cru (lower panel).

the variation in the temperature corresponding to the hard energy component could be the result of a variation in $N_{\rm H}^2$ (i.e. varying optical depth; see Section 1). This further supports the wind–wind collision phenomenon in these binaries.

4.2 X-ray temperatures of plasma

The X-ray spectra of WR binaries are well-defined by 2T plasmas. The values of log $(L_{\rm X}/L_{\rm bol})$ in the total energy band are found to be −6.6 and −7.2 for V444 Cyg and CD Cru, respectively. These values are similar to those for other WR (WN) stars observed from *XMM–Newton* and *Chandra* (Güdel & Nazé 2009). The temperatures of the cool components of WR binaries are comparable to those of other WR binaries: for example, 0.56–0.67 keV for WR1 (Ignace, Oskinova & Brown 2003) and 0.7–0.8 keV for WR 147 (Skinner et al. 2007). However, the temperatures corresponding to the hot energy components of these WR binaries are slightly more than those of some similar binaries. The possible mechanisms for the generation of X-rays are discussed below.

4.2.1 Instabilities in radiation-driven wind shocks

The wind-shock model predicts the intrinsic instability of the line driving mechanism. The standard model estimates the shock velocities by the relation $kT_{\rm sh} = 1.95\ \mu\ v_{\rm shock}^2$ (Lucy 1982; Luo et al. 1990). The temperatures of the cool energy components are found to be almost similar (∼0.6 keV) for both binary systems (see Tables 3 and 4). Adopting the mean particle weights $\mu \approx 1.16$ (Skinner et al. 2007) for WN stars and $\mu \approx 0.62$ for O-type stars (Cassinelli et al. 2008), we derived the 'average' value of shock velocities ≈515 km s^{-1} for WN stars and ≈704 km s^{-1} for O-type stars, corresponding to the cool component. These values are about a factor of 2 larger than those predicted by the radiative shock model of Lucy (1982). However, the advanced version of the wind-shock model by Owocki, Castor & Rybicki (1988) predicts X-ray emission up to 1 keV. Moreover, the temperatures of the cool energy component and $N_{\rm H}^{\rm l}$ do not vary with the orbital phase. Therefore, it appears that the cool energy components of V444 Cyg and CD Cru could be generated by either of the binary components and may be explained by instabilities in the radiation-driven wind shocks.

4.2.2 Magnetically confined wind shock

Babel & Montmerle (1997) have suggested that the presence of magnetic fields confines the wind, which may be an important ingredient for the production of X-ray emission. The degree of confinement of wind by the magnetic field is derived in terms of a confinement parameter $\Gamma = B_0^2 R_*^2/\dot{M} v_\infty$, where B_0 is the surface equatorial magnetic field strength (ud-Doula & Owocki 2002). For a confined wind model, $\Gamma \gg 1$. Using the values of stellar radius (R_*) and

stellar mass-loss rate ($\dot{M}v$) as given in Table 1 for the V444 Cyg binary components, the minimum magnetic field required to confine the wind is derived to be 0.14 kG for the primary and 1.25 kG for the secondary. Similarly, for CD Cru, we derived a minimum magnetic field of 0.16 and 1.96 kG for the primary and secondary components, respectively. Based on the formula given by Babel & Montmerle (1997) and using the above-estimated values of B, the X-ray luminosities are estimated to be $10^{34.66}$ and $10^{35.74}$ erg s^{-1} for the primary and secondary components of V444 Cyg, and $10^{35.06}$ and $10^{36.8}$ erg s^{-1} for the primary and secondary components of CD Cru. Such a high X-ray luminosity has not been observed for any WR binaries. However, smaller fields can exist and the confinement may be limited to just above the magnetic equatorial plane.

4.2.3 *Colliding wind-shock model*

Assuming that shock velocities have reached terminal velocities, the standard model predicts a maximum temperature for the shocked region from the winds of massive stars by the relation $kT_{\rm sh}^{\rm max} = 1.95\,\mu v_{\infty}^2$ (Luo et al. 1990). The nominal wind parameters of massive stars (see Table 1) and the mean particle weight μ for WN stars and for O-type stars give the maximum temperature generated by the individual components of binaries. The derived values are 7.80 + 7.21 keV for V444 Cyg (O6 + WN5) and 10.88 + 13.69 keV for CD Cru (O5 + WN6). The maximum observed temperature at phase 0.29 corresponding to the hot component is found to be similar to that of the maximum possible values for V444 Cyg. However, for CD Cru, the maximum observed temperature is less than that of the maximum possible values.

The phase-locked variability of the hard energy component shows that the observed hot X-ray temperatures in massive binaries could originate from the collision of stellar winds. The distances from the stars where these winds meet are derived using the relation (Stevens, Blondin & Pollock 1992; De Becker 2007):

$$r_{\rm OB} = \frac{1}{1+\eta^{1/2}} D. \quad (1)$$

Here, $r_{\rm OB}$ is the distance to the collision zone from the primary and D is the separation between the binary components. The wind momentum ratio η is expressed as

$$\eta = \frac{\dot{M}_2 v_{\infty,2}}{\dot{M}_1 v_{\infty,1}}, \quad (2)$$

where $y\dot{M}_1$ and $\dot{M}_2$ are the mass-loss rates of the primary and secondary components, respectively, and $v_{\infty,1}$ and $v_{\infty,2}$ are the terminal velocities of the primary and secondary components, respectively. Using the above relations, we have derived wind momentum ratios of 7.03 and 24.60 for V444 Cyg and CD Cru, respectively. The distances to the collision zone from the primary are estimated to be 0.27 and 0.17 times their corresponding binary separation (D) for V444 Cyg and CD Cru, respectively. Therefore, the collision zone is very close to the primary O-type star for both binaries. Furthermore, the collision wind zone will produce a bow shock around the O-type star, and the shock volume and the emission measure are dominated by WR winds; therefore, the X-ray emitting plasma also shows non-solar abundances.

The gas in a colliding wind region could be either adiabatic or radiative and depends upon the value of the cooling parameter (χ). This is defined as the ratio of the cooling time ($t_{\rm cool}$) of the shocked gas to the escape time ($t_{\rm esc}$) from the intershock region (Stevens et al. 1992):

$$\chi = \frac{t_{\rm cool}}{t_{\rm esc}} = \frac{v_3^4 d_{\dot{M}-7}}{.} \quad (3)$$

Here, v_3 is the pre-shock velocity in units of 10^3 km s^{-1}, d_7 is the distance from the stellar centre to the shock in units of 10^7 km and $\dot{M}_{-7}$ is the mass-loss rate in units of 10^{-7} M$_\odot$ yr^{-1}. Using the parameters given in Table 1 and the values from the above estimation, we derived cooling parameters χ_1 and χ_2 for the primary and secondary components, respectively. The estimated values of χ_1 and χ_2 are given Table 5. The winds from WR stars are found to be clearly radiative ($\chi < 1$) for both binaries. The intrinsic luminosity can be estimated for each component of the binary using the following relation (Pittard & Stevens 2002):

$$L_X = 0.5\Xi\dot{M}v^2. \quad (4)$$

Here, Ξ accounts for geometrical and inefficiency factors and v is the wind speed at the contact surface (i.e. pre-shock velocities derived from observed temperatures). The values of Ξ_1 (0.403 for V444 Cyg and 0.564 for CD Cru) and Ξ_2 (0.033 for V444 Cyg and 0.0042 for CD Cru) for the primary and secondary stars, respectively, are taken from Pittard & Stevens (2002). Table 5 gives the estimated values of the intrinsic luminosities of each component and the total intrinsic luminosities of the binary systems. These values are nearly three orders of magnitude higher than the observed values. Similar results have been found for other WR binaries, such as HD 159176 (De Becker et al. 2004) and WR 147 (Skinner et al. 2007). De Becker et al. (2004) suggested that the disagreement between observed and theoretical predictions could possibly be explained by the following: (i) the kinetic power of the collision

Table 5. Derived values of wind parameters and intrinsic luminosities for binary systems. The pre-shock velocities for each component are estimated using the derived values of post-shock temperatures.

Object Name	Phase	$v_{\rm pre-shock}$ km s^{-1}	χ_1	χ_2	log($L_{\rm X1}$) erg s^{-1}	log($L_{\rm X2}$) erg s^{-1}	log($L_{\rm total}$) erg s^{-1}
V444 Cyg	0.01–0.04	$2598^{+745}_{-779} + 1899^{+545}_{-570}$	5.496	0.416	$35.711^{+0.109}_{-0.155}$	$35.352^{+0.109}_{-0.155}$	$35.869^{+0.087}_{-0.109}$
	0.12–0.14	$1237^{+71}_{-90} + 904^{+52}_{-66}$	0.282	0.021	$35.067^{+0.024}_{-0.033}$	$34.708^{+0.024}_{-0.033}$	$35.224^{+0.021}_{-0.022}$
	0.27–0.30	$2819^{+475}_{-306} + 2061^{+347}_{-223}$	7.623	0.577	$35.782^{+0.068}_{-0.050}$	$35.423^{+0.068}_{-0.050}$	$35.940^{+0.043}_{-0.048}$
	0.38–0.41	$1735^{+226}_{-249} + 1269^{+165}_{-182}$	1.094	0.083	$35.361^{+0.053}_{-0.067}$	$35.002^{+0.053}_{-0.067}$	$35.518^{+0.043}_{-0.048}$
	0.45–0.50	$1632^{+164}_{-89} + 1193^{+120}_{-65}$	0.856	0.065	$35.307^{+0.042}_{-0.024}$	$34.948^{+0.042}_{-0.024}$	$35.465^{+0.025}_{-0.026}$
	0.50–0.51	$1276^{+1242}_{-358} + 933^{+908}_{-262}$	0.320	0.024	$35.094^{+0.295}_{-0.143}$	$34.735^{+0.295}_{-0.143}$	$35.252^{+0.169}_{-0.281}$
CD Cru	0.01–0.09	$1879^{+861}_{-632} + 1374^{+630}_{-462}$	0.990	0.047	$35.798^{+0.164}_{-0.178}$	$34.875^{+0.164}_{-0.178}$	$35.847^{+0.133}_{-0.192}$
	0.43–0.51	$1224^{+101}_{-102} + 895^{+74}_{-75}$	0.178	0.008	$35.425^{+0.034}_{-0.038}$	$34.502^{+0.034}_{-0.038}$	$35.474^{+0.031}_{-0.034}$
	0.73–0.83	$1161^{+633}_{-85} + 849^{+462}_{-62}$	0.144	0.007	$35.380^{+0.189}_{-0.033}$	$34.457^{+0.189}_{-0.033}$	$35.428^{+0.107}_{-0.141}$

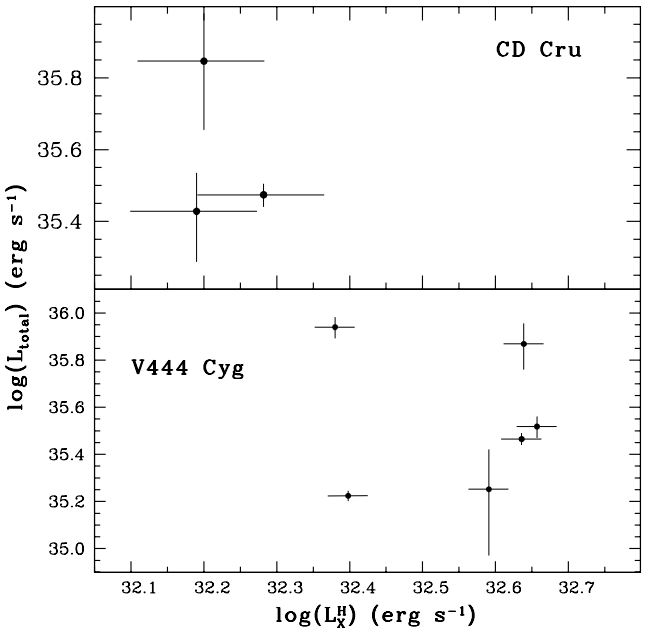

Figure 8. Observed versus model X-ray luminosity.

should be considered as an upper limit on the X-ray luminosity; (ii) a higher value of the parameter η should be considered; (iii) diffusive mixing between hot and cool material is likely to exist because of the instability of the shock front; (iv) orbital effects should also be included to study such systems. The observed and theoretically predicted values of X-ray luminosities are shown in Fig. 8. This model also predicts the phase-locked variations that can be seen in Fig. 6. Therefore, it appears that the hard energy component is most likely associated with the wind collision zone.

4.2.4 Non-thermal emission

There is no strong justification for invoking a non-thermal origin of X-ray emission as the observed X-ray emission at higher energies can be fitted satisfactorily with a thermal model (see Figs 4 and 5). However, the present data are limited up to 10 keV and it is difficult to eliminate the contribution of non-thermal components from the spectra. These are dominated by the presence of strong thermal emission, and the non-thermal emission is overwhelmed by the thermal emission (De Becker 2007). Therefore, we can state that the spectra of massive stars in the present sample are fairly well explained by 2T plasma models.

5 SUMMARY

We have analysed the X-ray temporal and spectral properties of two WR binaries, V444 Cyg and CD Cru, observed with high-sensitivity EPIC instruments on board the *XMM–Newton* satellite. The X-ray light curves in the soft and hard energy bands show the phase-locked variability. Both primary and secondary minima were seen in the hard band X-ray light curves of both binaries. However, in the soft X-ray light curve only the primary minimum was seen. This implies that the hard energy component could be originating from the wind–wind collision zone. The X-ray spectra of both WR binaries show strong absorption below $\approx$1 keV and clear evidence of high-temperature plasma, manifested by a visible Fe K α emission-line complex. The study of the X-ray spectra reveals cool as well as hot temperature plasma components of binary stars, which are fitted consistently with 2T plasma models. The cooler plasma component was found to be constant at all phases with a mean value of $\sim$0.6 keV for both binaries. The presence of a cooler component could be a result of the distribution of small-scale shocks in the radiation-driven outflows from either the primary or the secondary star in the binary systems. The temperature of the hot plasma component and the corresponding column density were found to be variable during the orbital cycle of both binaries. The variation in temperature of hot plasma could be because of the varying circumstellar optical depth along the line of sight towards the shock as the stars revolve around each other. The maximum value of the hot plasma was found to be lower than the hottest plasma possible in the binary systems as predicted by colliding wind theory for short-period binaries. However, the predicted values of X-ray luminosities are $\sim$ three orders of magnitude more than the observed values and cannot be accounted for in terms of observational errors.

ACKNOWLEDGMENTS

We thank the referee, Dr Marc Gagné, for his useful suggestions. We would like to thank Dr Maheshwar Gopinathan for a critical reading of the manuscript. This publication makes use of data products from the *XMM–Newton* archives using the High-Energy Astrophysics Science Archive Research Center, which has been established at Goddard by NASA. We acknowledge the *XMM–Newton* Help Desk for their remarkable support with the X-ray data analysis. In this research we have also made use of the Simbad and VizieR catalogue data access tool, CDS, Strasbourg, France.

REFERENCES

Albacete Colombo J. F., Méndez M., Morrell N. I., 2003, MNRAS, 346, 704
Antokhin I. I., 2007, Astron. Astrophys. Trans., 26, 59
Antokhin I. I., Owocki S. P., Brown J. C., 2004, ApJ, 611, 434
Babel J., Montmerle T., 1997, A&A, 323, 121
Balucińska-Church M., McCammon D., 1992, ApJ, 400, 699
Berghöfer T. W., Schmitt J. H. M. M., Danner R., Cassinelli J. P., 1997, A&A, 322, 167
Borkowski K. J., Lyerly W. J., Reynolds S. P., 2001, ApJ, 548, 820
Broos P. S., Feigelson E. D., Townsley L. K., Getman K. V., Wang J., Garmire G. P., Jiang Z., Tsuboi Y., 2007, ApJ, 169, 353
Cassinelli J. P., Ignace R., Waldron W. L., Cho J., Murphy N. A., Lazarian A., 2008, ApJ, 683, 1052
Cherepashchuk A. M., Karetnikov V. G., 2003, Astron. Rep., 47, 38
Cherepashchuk A. M., Eaton J. A., Khaliullin Kh. F., 1984, ApJ, 281, 774
Corcoran M. F., Stevens I. R., Pollock A. M. T., Swank J. H., Shore S. N., Rawley G. L., 1996, ApJ, 464, 434
De Becker M., 2007, A&AR, 14, 171
De Becker M., Rauw G., Pittard J. M., Antokhin I. I., Stevens I. R., Gosset E., Owocki S. P., 2004, A&A, 416, 221
Ehle M. et al., 2004, User Guide to the *XMM–Newton* Science Analysis System, http://xmm.vilspa.esa.es
Gagné M., Oksala M. E., Cohen D. H., Tonnesen S. K., ud-Doula A., Owocki S. P., Townsend R. H. D., MacFarlane J. J., 2005, ApJ, 628, 986
Güdel M., Nazé Y., 2009, A&AR, 17, 309
Ignace R., Oskinova L. M., Brown J. C., 2003, A&A, 408, 353
Khaliullin Kh. F., Khaliullina A. I., Cherepashchuk A. M., 1984, SvAL, 10, 250 (also published as AJ, 18, 229)
Kudritzki R.-P., Puls J., 2000, ARA&A, 38, 613
Kurosawa R., Hillier D. J., Pittard J. M., 2002, A&A, 388, 957
Lamontagne R., Moffat A. F. J., Drissen L., Robert C., Matthews J. M., 1996, AJ, 112, 2227

Leutenegger M. A., Kahn S. M., 2003, ApJ, 585, 1015
Lodders K., 2003, ApJ, 591, 1220
Lucy L. B., 1982, ApJ, 255, 286
Lucy L. B., White R. L., 1980, ApJ, 241, 300
Luo D., McCray R., Mac Low M., 1990, ApJ, 362, 267
Maeda Y., Koyama K., Yokogawa J., Skinner S., 1999, ApJ, 510, 967
Marchenko S. V., Moffat A. F. J., Eenens P. R. J., Cardona O., Echevarria J., Hervieux Y., 1997, ApJ, 485, 826
Massey P., Johnson K. E., Degioia-Eastwood K., 1995, ApJ, 454, 151
Moffat A. F. J., 1974, A&A, 34, 29
Moffat A. F. J., Firmani C., McLean I. S., Seggewiss W., 1982, in de Loore C. W. H., Willis A. J., eds, Proc. IAU Symp. 99, Wolf–Rayet Stars: Observations, Physics, Evolution. Reidel, Dordrecht, p. 577
Moffat A. F. J. et al., 1990, ApJ, 350, 767
Münch G., 1950, ApJ, 112, 266
Nazé Y., Corcoran M. F., Koenigsberger G., Moffat A. F. J., 2007, ApJ, 658, 25
Niemela V. S., Massey P., Conti P. S., 1980, ApJ, 241, 1050
Nugis T., Lamers H. J. G. L. M., 2000, A&A, 360, 227
Owocki S. P., Cohen D. H., 1999, ApJ, 520, 833
Owocki S. P., Castor J. I., Rybicki G. B., 1988, ApJ, 335, 914
Piatti A. E., Bica E., Santos J. F. C. Jr, Clariá J. J., 2002, A&A, 387, 108
Pittard J. M., Stevens I. R., 2002, A&A, 388, 20
Pollock A. M. T., 1987, AJ, 320, 283
Rauw G., 2008, RevMexAA Ser. Conf., 33. 59
Repolust T., Puls J., Herrero A., 2004, A&A, 415, 349
Sagar R., Munari U., de Boer K. S., 2001, MNRAS, 327, 23
Sana H., Rauw G., Nazé Y., Gosset E., Vreux J.-M., 2006, MNRAS, 372, 661
Schaifers K., Voigt H. H., 1982, Numerical Data and Functional Relationships in Science and Technology, New series, Group VI, Vol. 2b. Springer-Verlag, Berlin
Skinner S. L., Zhekov S. A., Güdel M., Schmutz W., 2007, MNRAS, 378, 1491
Smith R. K., Brickhouse N. S., Liedahl D. A., Raymond J. C., 2001, ApJ, 595, 365
Stelzer B., Flaccomio E., Montmerle T., Micela G., Sciortino S., Favata F., Preibisch T., Feigelson E. D., 2005, ApJ, 160, 557
Stevens I. R., Blondin J. M., Pollock A. M. T., 1992, ApJ, 386, 265
Strüder L. et al., 2001, A&A, 365, 18
Turner M. J. L. et al., 2001, A&A, 365, 27
ud-Doula A., Owocki S. P., 2002, ApJ, 576, 413
Underhill A. B., Fahey R. P., 1987, ApJ, 313, 358
Underhill A. B., Grieve G. R., Louth H., 1990, PASP, 102, 749
Usov V. V., 1992, ApJ, 389, 635
van der Hucht K. A., 2001, NewAR, 45, 135
van der Hucht K. A., Conti P. S., Lundstrom I., Stenholm B., 1981, Space Sci. Rev., 28, 227
Vuong M. H., Montmerle T., Grosso N., Feigelson E. D., Verstraete L., Ozawa H., 2003, A&A, 408, 581

This paper has been typeset from a TEX/LATEX file prepared by the author.